www.nature.com/scientificdata

scientific data

OPEN

DATA DESCRIPTOR

Brain MRI Dataset Featuring a Full Clinical Protocol With and Without Intentional Motion

Kathrine Skak Madsen[1], Tim Ruschke[2,3], Hannah Eichhorn[4,5], Puk Rising[2] & Melanie Ganz[2,3] ✉

Motion-induced artefacts in MRI are a common occurrence but can obscure pathologies or be falsely identified as pathological. Reacquiring motion-corrupted scans is expensive, and thus retrospective and prospective motion correction methods have been introduced. Although motion correction shows promise, there is a lack of exhaustive testing on its efficacy with respect to full clinical cerebral MRI protocols. Here we present a dataset ($n = 22$) to facilitate future research, which includes data with and without intentional motion, and with and without prospective motion correction, across six MRI sequences included in a full clinical cerebral MRI protocol. Motion was captured by an external tracking device, and the dataset includes the motion data as derived motion transforms. For standardization, all image data are fully BIDS-compliant. Raw k-space data are available as well. As the dataset pairs motion-free data with motion-corrupted data, it can be used to develop or test different motion-correction or k-space reconstruction methods.

Background & Summary

Magnetic Resonance Imaging (MRI) is widely used in clinical as well as research settings due to its non-invasiveness and excellent soft tissue contrast. Nevertheless, it suffers from some drawbacks. One drawback is the time required to complete an imaging sequence, which is in the magnitude of minutes[1]. Since imaging is a gradual process, motion during the scanning can causes artefacts in the final image, such as ghosting or blurring. These artefacts in turn hamper the diagnostic potential as they can obscure pathologies or lead to false positives when unaddressed[1–3]. In addition to involuntary and unavoidable movements such as breathing, movement can occur as a result of discomfort or a myriad of other reasons. Children are especially prone to movement, with nodding being one of the most common patterns[4]. Scans identified as inadequate can be reacquired, but this requires additional time and incurs financial costs[5].

Several different methods have been developed in the literature to address motion-induced artefacts. Motion can be reduced by targeting the patient behavior, such as by familiarizing children to the scanner environment beforehand[6] or sedating them with general anasthesia (GA)[7]. However, GA is associated with increased costs[5] and may pose health risks to the developing brain[8]. Besides trying to reduce motion physically during acquisition, one can also try to address motion algorithmically. Here, prospective motion correction constitutes one approach. It alters the imaging process itself by aiming to correct for motion during scan acquisition. For example, by tracking the movement of the patient through an external device, it is possible to adjust the field of view of the scanner accordingly and thereby counteract the movement of the patient[9–11]. Due to the nature of prospective motion correction, there is no original image with which to compare, which can make it difficult to quantify its impact. Lastly, selective reacquisition forgoes acquiring an entirely new scan and instead only reacquires those parts of the k-space with the highest motion, which translates to improved image quality[12–14]. Selective reacquisition can also be combined with prospective motion correction.

Retrospective motion correction constitutes another algorithmic approach, aiming to correct the image after the acquisition, which can take the form of classical algorithms[15,16] or neural networks[17,18]. Retrospective motion

[1]Danish Research Centre for Magnetic Resonance, Department of Radiology and Nuclear Medicine, Copenhagen University Hospital - Amager and Hvidovre, Hvidovre, Denmark. [2]Neurobiology Research Unit, Copenhagen University Hospital - Rigshospitalet, Copenhagen, Denmark. [3]Department of Computer Science, University of Copenhagen, Copenhagen, Denmark. [4]Institute of Machine Learning in Biomedical Imaging, Helmholtz Munich, Neuherberg, Germany. [5]School of Computation, Information and Technology, Technical University of Munich, Munich, Germany. ✉e-mail: melanie.ganz@nru.dk

correction based on supervised learning requires paired data on which the algorithm can train. Unfortunately, data with realistic motion paired with motion-free ground-truth scans are rare, particularly in combination with qualitative evaluation of the scan quality, as its acquisition is costly[17]. Note, by realistic motion we here refer to the fact that the motion is actually happening during MRI acquisition and not simulated post-hoc. While datasets that contain motion-degraded data have been shared[19], those datasets were limited in the sense that they only share the images and motion scores, but not the ground truth motion measured by an external device. This lack of readily available training data motivates alternatives like unsupervised approaches, but testing the quality of these approaches still often requires paired data. Furthermore, many retrospective motion correction techniques require raw k-space data[20], which are rarely available. While there exist previous datasets like the fastMRI dataset[21] that include k-space data measurements, the fastMRI dataset is also lacking paired motion-free and motion-corrupted data and requires manual selection of motion-corrupted cases. Currently, there is a lack of k-space datasets with real motion, and hence researchers often rely on simulated motion or using magnitude-only datasets.

Our dataset consists of healthy adults recruited for the Cimbi database[22]. Images available include a full clinical cerebral MRI protocol, albeit with some sequences only available for a subset of all patients. Each sequence was acquired with and without intentional motion, as well as with and without prospective motion correction (PMC), resulting in ground-truth (motion-free) data paired with realistically motion-degraded data and prospectively corrected data. The data are structured according to the BIDS format[23], an open standard for structuring MRI data to facilitate its sharing. The image data are published on the platform OpenNeuro[24], a free and open platform for sharing BIDS-compliant MRI data (among others), while the raw k-space data is published on PublicnEUro (https://publicneuro.eu/), a EU General Data Protection Regulation (GDPR) compatible data sharing site where data can only be shared under data usage agreement (DUA). The optical tracking system Tracoline (TracInnovations, Ballerup, Denmark)[25,26] was used for PMC. With this dataset of paired image and raw MRI data with and without motion-artefacts, we aim to facilitate future development and validation of retrospective motion correction algorithms. Hence, the main advantage of the presented dataset is for developing and validating new retrospective motion correction and specifically motion-robust reconstruction algorithms in the future. Additionally, we also share image quality observer scores by a neuroradiologist and two radiographers. The image quality scores together with the images with and without prospective motion correction can serve as a basis of e.g., developing image quality metrics.

The dataset has previously been used to investigate the effects of motion correction and selective reacquisition on brain MRI for a full clinical protocol in healthy adults[27,28]. The analysis showed improvements in image quality for retrospective motion correction and significant improvements for prospective motion correction in combination with selective reacquisition. The code is available on github at https://github.com/melanieganz/MoCoProject/tree/main/MotionCorrectedClinicalMRProtocol. As the data pair realistic motion-induced artefacts with motion-free images, the data may for example be re-used to test the quality of different motion-correction or k-space reconstruction methods, which was encouraged by the RealNoiseMRI challenge[29] in 2021.

Methods

Participants. Twenty-two healthy adults (16 females, 6 males) aged 19 to 36 years (mean and standard deviation: 23.5 ± 4.3 years) were recruited for the Cimbi database[22]. Data acquisition lasted from January to March 2021. Ethical approval was obtained from the Ethics Committees for the Capital Region of Denmark (protocol number H-KF-2006-20). Written informed consent was obtained from all participants before initiation of study procedures.

Clinical MRI protocol. Participants were scanned with a 3T Siemens Magnetom Prisma scanner using a 64-channel head coil (Siemens Healthcare GMBH, Erlagen, Germany) at Copenhagen University Hospital (Rigshospitalet, Copenhagen, Denmark). The data encompass six different MRI sequences typically included in a pediatric clinical cerebral protocol. Not all sequences are available for each subject, since some of the PMC sequences were only developed during the course of our study or needed to be re-compiled for the software version we were operating on. Specifically, the protocol included: a 3D T1-weighted Magnetization Prepared Rapid Gradient Echo (T1 MPR) ($n = 22$), 3D T2-weighted Dark Fluid (Fluid-Attenuated Inversion Recovery) (T2 FLAIR) ($n = 10$), 2D T1-weighted Short-TI Inversion Recovery (T1 STIR) ($n = 22$), 2D T2-weighted Turbo Spin Echo (T2 TSE) ($n = 22$), 2D T2*-weighted Gradient Echo (T2* GRE) ($n = 19$) and 2D diffusion weighted imaging (DWI) ($n = 10$). The sequences were compiled for software version syngo MR E11. For more details on each sequence, see Table 1. For the full sequence information see supplementary material (section 3).

Prospective motion correction was based on the motion estimated by an external motion tracking system and executed by adjusting the scanner's field of view following the approach described in[10]. The timing and frequency of the updates differed between sequences, but the position update frequency of the tracking is approx. 30 ms/30Hz. For the 3D T1 MPR, correction was applied within echo train (ET) as it allowed for 5–6 updates during the echo time, while for the 3D T2 FLAIR updates were applied before ET[10], and for all 2D sequences updates were applied before each slice excitation.

With the exception of the DWI and T2* GRE sequences, each scan with intentional motion included selective reacquisition, which involves reacquiring a fixed number of k-space lines with the highest detected motion based on the motion tracking data. Scans were then reconstructed both with and without the reacquired lines. If a reacquired line displayed higher motion than the original one, the original was used instead.

	T1 MPR	T2 FLAIR	T1 STIR	T2 TSE	T2* GRE	DWI	Cross Calibration
TR[1] [ms]	2000	5000	4100	4010	700	3200	5.4
TI[2] [ms]	900	1800	1600	—	—	—	—
TE[3] [ms]	2.32	3.88	8.5	116	20	79	2.44
α^4 [°]	8.0	variable	150	150	20	90	6.0
Voxel size [mm]	0.9^3	1.0^3	$0.9 \times 0.9 \times 5.0$	$0.4 \times 0.4 \times 5.0$	$0.5 \times 0.5 \times 5.0$	$1.7 \times 1.7 \times 4.0$	2.0^3
Orientation	sagittal	sagittal	transversal	transeversal	transversal	transversal	coronal
PE[5] direction[6]	$A \rightarrow P$	$A \rightarrow P$	$R \rightarrow L$	$R \rightarrow L$	$R \rightarrow L$	$A \rightarrow P$	$R \rightarrow L$
Acceleration Factor PE	2	3	2	2	—	2	2
Scan duration	5m 12s	4m 12s	3m 51s	3m6s	2m 25s	42s	17s
Reacquisition	16 TR	7 TR	10 TR	9 TR	—	—	—

Table 1. Details of the MRI Sequences used, including the cross calibration step that is used for converting the Tracoline coordinate system to the scanner coordinate system. Note, the T1 STIR and T2 TSE sequences were acquired interleaved. Reproduced with permission from[27]. [1]Repetition Time. [2]Inversion Time. [3]Echo Time. [4]Flip angle α. [5]Phase Encoding. [6]A = Anterior, P = Posterior, R = Right, L = Left.

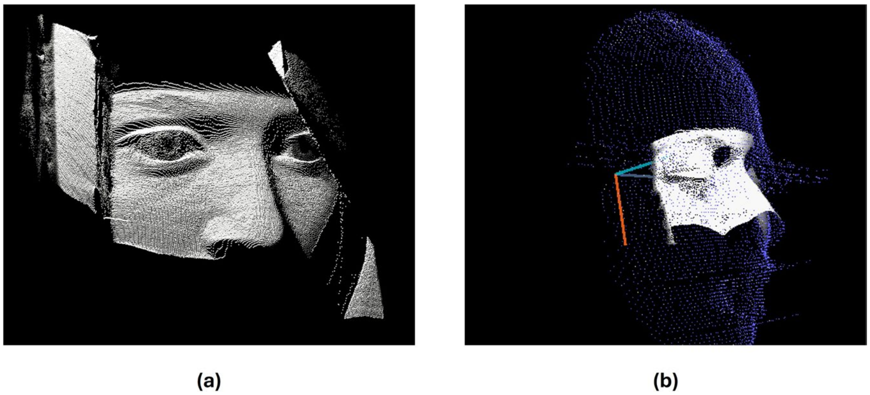

Fig. 1 (**a**) Point cloud example visualizing the camera field of view of a subject within the head coil. (**b**) Cross calibration between face selective MR scan (blue) and Tracoline point cloud (white). Figure reproduced with permission from[27].

Scan Instructions. Participants were instructed in three different motion patterns: still, nodding, and shaking. Still and nodding scans are available for all sequences, while shaking was limited to the T1 MPR sequence only. Further, for each motion pattern, we acquired two scans, one with prospective motion correction and one without. The choice of nodding as the main motion pattern was based on previous research[4] showing that the most common rotational movement in children's MRI is a nodding motion.

Several methods were introduced in an effort to increase consistency across participants. First, each participant was trained before the scan to keep the motion amplitude (measured by camera coordinates) in a constant range between 8 and 15 mm for the nodding pattern, and between 12 and 20 mm for the shaking pattern. Next, motion was divided into sub-positions spaced 5 seconds apart. During the scan, the participants were guided through the motion by being told the time every 5 seconds. For this purpose, the nodding motion was divided into the following series of positions: center, top, center, bottom, center. Lastly, the constant movement range was further reinforced by stickers in the scanner bore indicating the range of the three positions: top, center, and bottom. Scans were retaken if the motion range significantly exceeded the intended range.

While the motion curves can be viewed to examine the patient-wise motion trajectories, there were some general rules followed for each participant: All motions were for all sequences always started at the same time during the different acquisitions. For the two 3D sequences, the motion of the volunteer was placed in the centre of the k-space acquisition and lasted for 40 seconds, corresponding to two periods of a sinusoid motion with the 5-second instructions via the intercom as described above. For the 2D sequences that were partially acquired interleaved, the motion was started during the first of the acquisition passes. Motion was of the same length as for the 3D sequences, covering almost all of the slices acquired during the first interleaved acquisition pass.

Motion tracking system. Motion tracking was performed using the markerless optical tracking system Tracoline (TracInnovations, Ballerup, Denmark)[25,26]. Tracoline emits invisible infra-red light on the patient's face, which is used to generate a point cloud via a synchronized camera that picks up the reflected light. Approx. 30 point clouds are generated each second. The latency between pose estimation and updating the scanner's field of view lies between 60 and 110 ms[10]. Figure 1(a) shows a point cloud recorded by the tracking system.

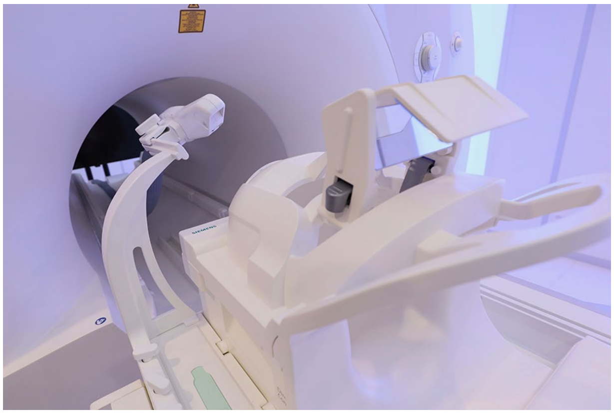

Fig. 2 Tracoline camera on the scanner bed.

Motion type	RMS displ. [mm]	Median displ. [mm]	Maximum displ. [mm]
Still (mean ± std)	0.64 ± 0.55	0.54 ± 0.55	1.3 ± 1.1
Nodding (mean ± std)	3.3 ± 3.0	1.7 ± 2.7	13.1 ± 5.2

Table 2. The level of motion added by intentional movement can be quantified by calculating displacement metrics over all sequences.

Since Tracoline and the scanner each have their own coordinate system, converting one into the other requires an additional cross calibration step. This involves a short additional MRI scan (see cross calibration in Table 1) of the subject's face, which the Tracoline software can then use to calculate a conversion matrix through an iterative closest point algorithm between the point cloud and the facial surface extracted from the MRI scan[10]. Figure 1(b) shows the cross-calibration step. The integration of the Tracoline system into the scanner is visualized in Fig. 2. For more details, regarding Tracoline usage, see supplementary material (section 1).

Data Records

All imaging and motion tracking data are published on OpenNeuro[24]. Since the image data shared on OpenNeuro is considered fully anonymized, we can share this data under public service as a legal basis as recognized by the Danish Data authority following GDPR. Please note that all imaging data needs to be defaced prior to upload to OpenNeuro and this was done using pydeface (https://pypi.org/project/pydeface/). Data are organized according to the BIDS standard[23], which defines, among other rules and guidelines, a consistent folder structure, as well as file name patterns and formats. The data was converted using dcm2niix (https://github.com/rordenlab/dcm2niix) and local MatLab scripts. At the top-level, the *participants.tsv* lists all patients along with the additional meta-data of sex and age and is further described by the *participants.json* file. The file *dataset_description.json* contains descriptive information about the dataset.

Volunteers are identified as subjects and ordered into separate folders (designated by *sub-01* etc.). The scans of all sequences are then located in the nested *anat* (anatomical) folder, including an associated sidecar json-file with the same name as the scan, which contains meta-data. The only exception to this is the diffusion-weighted data (DWI-suffix) consisting of ADC and TRACEW images. We included the DWI data in the *derivatives* folder under the subfolder *clinical_dwi*. From there, the folder structure follows the same pattern as before, one folder for each volunteer. While we consider this data derived even if there is no pipeline due to being generated at the scanner, we point out that this data is so far not strictly standardized by BIDS and thus multiple approaches are possible. We still follow the same BIDS pattern as the other data when it comes to file-names, and due to the ADC and TRACEW images being clinically used like the other sequences, we also nest the data in an *anat* subfolder. All images are NIfTI files.

Additionally, observer scores can be found in *derivatives* under *observer_scores* for FLAIR, MPRAGE, T1 TIRM and T2 TSE, with an additional ranking for the DWI data. File names are shortened versions of the BIDS filename of a scan for their respective sequence. For each sequence, there is a TSV file containing the score/ranking for each subject and subsequence (with/ without PMC, etc.) paired with a sidecar .json file (with the same name) that explains the columns. This follows the same pattern as *participants.tsv* and *participants.json*. The *derivative* folder also contains the processed data under *freesurfer*. Lastly, the Tracoline motion data is located under the top level folder *source*, again organized into subject folders. The files provided in each subfolder are all Tracoline tracking files. Here, it is noteworthy that the .tsm file contains the 3D motion with the default cross calibration, used e.g. for motion statistics such as in the brainmrimotion.org database. For usage for motion correction one needs to use the .poa file with the actual rotation matrices and the .aln files. For detailed usage, please see[27].

Lastly, the raw k-space data are published on the GDPR compatible data sharing site PublicnEUro https://publicneuro.eu/ and available at[30]. Data are also organized according to the BIDS standard[23]. At the top-level, the *participants.tsv* lists all patients along with the additional meta-data of sex and age and is further described by the *participants.json* file. The file *dataset_description.json* contains descriptive information about the dataset.

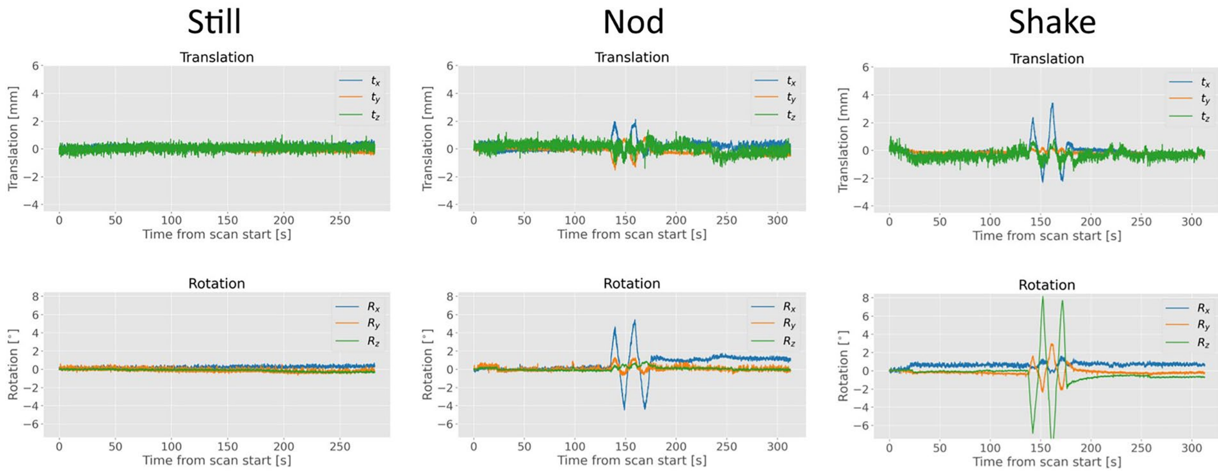

Fig. 3 Example of motion curves (translation and rotation) for each dimension and each motion type in the data. Example scans are T1 MPR. Please note the decomposed 3D motion shown here is the Euclidean distance of the point cloud centroid relative to the starting position. Figure reused with permission from[27].

Score	Description
5	Perfect scan without artefacts
4	Mild artefacts, but fully diagnostic
3	Mild to moderate artefacts. If an abnormality was noticed, it would be repeated.
2	Substantial artefacts. Large abnormalities can be discerned, but scan still needs to be repeated.
1	Completely non-diagnostic.

Table 3. Quality scores used by observers based on the Likert score. Ranges from 1 (non-diagnostic) to 5 (perfect).

The actual raw data are inside a source folder and distributed in ISMRM-RD format (see https://ismrmrd.github.io/apidocs/1.5.0/ for more details). Note that these data are not available on OpenNeuro as they cannot be considered fully anonymous (since the 3D k-space data cannot be defaced) and are therefore subject to a DUA.

Technical Validation

Quantifying the Motion. While we have previously described the methods by which motion was introduced into the scans, we also quantified the motion with concrete metrics to measure consistency across scans and the intensity of movement added relative to the still scans. The chosen metrics were root mean squared (RMS) as well as maximum and median displacement. Displacement was measured via euclidean distance of the point cloud centroid relative to the starting position. The results can be seen in Table 2. For motion during a concrete example scan, see Fig. 3.

Registration and Analysis. Validating image quality in[28] required registering images to the same space, the results of which are included in the dataset. The still, uncorrected scan for each respective sequence was considered the ground truth reference image to which the other scans (of the same participant and sequence) were registered. The registration process began with the extraction of a brain-mask using FreeSurfer[31] version 7.1.1. The brain masks were manually inspected and corrected according to FreeSurfer guidelines in case of errors. Then, using the FreeSurfer algorithm *bbregister*[32] for T1 MPR and *robust_register*[33] for other sequences, all other images were registered to the reference brain mask. Example images with and without motion and with and without prospective motion correction, including the associated motion graphs, are displayed in the supplementary material (section 2) for their respective sequence.

Observer scores. To validate and gauge the quality of the data, and in particular as a point of comparison between corrected and uncorrected data, the dataset includes a qualitative assessment by experts. Concretely, scans were scored based on an ordinal rating system from 1 to 5 which is modeled after the Likert scale in[34] (also see Table 3). Assessment was performed by one radiologist with 8 years of experience in (neuro-)radiology and two radiographers (recently graduated), providing three scores for each image. Observers were blinded to motion type and correction setting of each image. Note, observer scores are only available for T1 MPR, T2 FLAIR, T1 STIR, and T2 TSE sequences. The observer scores can be seen in Table 4.

For the DWI data, the approach for qualitative assessment was changed because differences between images were subtle and only recognizable in direct comparison. Instead of scoring, the radiologist instead ranked the four types of images (with/without PMC, still/nodding) from 1 to 4 (4 being the highest quality). The ranking

Motion	PMC	Reacquisition	T1 MPR	T2 FLAIR	T2 TSE	T1 TIRM
Still	no	No	4.96	4.70	3.94	4.20
Still	yes	No	4.77	4.28	4.35	3.93
Nodding	no	No	2.33	2.20	2.17	1.92
Nodding	no	Yes	3.06	3.30	2.63	2.97
Nodding	yes	No	3.68	2.93	2.93	2.72
Nodding	yes	Yes	4.32	3.73	3.48	3.30

Table 4. Observer scores for different sequences and combinations of prospective motion correction (PMC), intentional motion and reacquisition. Scores are the mean for all participants available for the sequence. Scores are weighted averages of the two radiographer scores and the radiologist score, with the radiologist's score being weighed twice as much as one radiographer's score.

was only performed by the neuroradiologist, not the radiographers, due to the limited experience of the radiographers with this modality. The assessment was based on the TRACEW images and ADC maps with both weighted equally Table 4.

Data availability

All imaging and motion tracking data are published on OpenNeuro[24]. Since the image data shared on OpenNeuro is considered fully anonymized, we can share this data under public service as a legal basis as recognized by the Danish Data authority following the GDPR (see details on https://commission.europa.eu/law/law-topic/data-protection/data-protection-explained_en). The k-space data presented can be viewed and browsed on[30] for assessment. Since they are considered personal data in order to download the data, one must register on publicneuro.eu (https://datacatalog.publicneuro.eu/manage/register), where IDs are verified (depending on user availability, expect a 1-day to 1-week delay). Once ID is verified, users can request data. For this dataset, a DUA must be signed and re-uploaded, and approval from the data controller's legal team is required (1-2 weeks). Sharing under DUA for neuroscientific research is in line with the ethics approval for the project under which this data was acquired. The DUA is also listed on the dataset webpage page for convenience. Note that for users outside the EU or adequacy countries, institutional signing of EU standard contractual clauses is also mandatory by EU law (as can be accessed here https://commission.europa.eu/law/law-topic/data-protection/international-dimension-data-protection/standard-contractual-clauses-scc_en). After the documents are signed and approved, users receive a link to the data for download via browser or command line.

Code availability

The code used for technical validation, registration, and generation of the figures used in this paper is openly available at https://github.com/melanieganz/MoCoProject/tree/main/MotionCorrectedClinicalMRProtocol. The repository also contains code used for analysis of the data and figures from[28] and[27]. The README files in the repository contain additional information on how to run the code.

Received: 16 July 2025; Accepted: 26 March 2026;
Published online: 23 April 2026

References

1. Godenschweger, F. *et al.* Motion correction in MRI of the brain. *Physics in medicine and biology* **61**, R32 (2016).
2. Zaitsev, M., Maclaren, J. & Herbst, M. Motion Artefacts in MRI: a Complex Problem with Many Partial Solutions. *Journal of magnetic resonance imaging : JMRI* **42**, 887 (2015).
3. Afacan, O. *et al.* Evaluation of motion and its effect on brain magnetic resonance image quality in children. *Pediatric Radiology* **46**, 1728–1735 (2016).
4. Eichhorn, H. *et al.* Characterisation of children's head motion for magnetic resonance imaging with and without general anaesthesia. *Frontiers in Radiology* **1**, 789632 (2021).
5. Slipsager, J. M. *et al.* Quantifying the Financial Savings of Motion Correction in Brain MRI: A Model-Based Estimate of the Costs Arising From Patient Head Motion and Potential Savings From Implementation of Motion Correction. *Journal of magnetic resonance imaging: JMRI* **52**, 731–738 (2020).
6. de Bie, H. M. A. *et al.* Preparing children with a mock scanner training protocol results in high quality structural and functional MRI scans. *European Journal of Pediatrics* **169**, 1079–1085 (2010).
7. Runge, S. B., Christensen, N. L., Jensen, K. & Jensen, I. E. Children centered care: Minimizing the need for anesthesia with a multi-faceted concept for MRI in children aged 4-6. *European Journal of Radiology* **107**, 183–187 (2018).
8. Stratmann, G. Review article: Neurotoxicity of anesthetic drugs in the developing brain. *Anesthesia and Analgesia* **113**, 1170–1179 (2011).
9. Zaitsev, M., Dold, C., Sakas, G., Hennig, J. & Speck, O. Magnetic resonance imaging of freely moving objects: Prospective real-time motion correction using an external optical motion tracking system. *Neuroimage* **31**, 1038–1050 (2006).
10. Frost, R. *et al.* Markerless high-frequency prospective motion correction for neuroanatomical MRI. *Magnetic Resonance in Medicine* **82**, 126–144 (2019).
11. van Niekerk, A., van der Kouwe, A. & Meintjes, E. Toward "plug and play" prospective motion correction for MRI by combining observations of the time varying gradient and static vector fields. *Magnetic Resonance in Medicine* **82**, 1214–1228 (2019).
12. Tisdall, M. D. *et al.* Volumetric navigators for prospective motion correction and selective reacquisition in neuroanatomical MRI. *Magnetic Resonance in Medicine* **68**, 389–399 (2012).
13. White, N. *et al.* PROMO: Real-time prospective motion correction in MRI using image-based tracking. *Magnetic Resonance in Medicine* **63**, 91–105 (2010).
14. Frost, R. *et al.* Prospective motion correction and selective reacquisition using volumetric navigators for vessel-encoded arterial spin labeling dynamic angiography. *Magnetic Resonance in Medicine* **76**, 1420–1430 (2016).
15. Atkinson, D., Hill, D., Stoyle, P., Summers, P. & Keevil, S. Automatic correction of motion artifacts in magnetic resonance images using an entropy focus criterion. *IEEE Transactions on Medical Imaging* **16**, 903–910 (1997).

16. Pipe, J. G. Motion correction with PROPELLER MRI: Application to head motion and free-breathing cardiac imaging. *Magnetic Resonance in Medicine* **42**, 963–969 (1999).
17. Spieker, V. *et al*. Deep learning for retrospective motion correction in mri: A comprehensive review. *IEEE Transactions on Medical Imaging* **43**, 846–859 (2024).
18. Usman, M., Latif, S., Asim, M., Lee, B.-D. & Qadir, J. Retrospective Motion Correction in Multishot MRI using Generative Adversarial Network. *Scientific Reports* **10**, 4786 (2020).
19. Nárai, Á. *et al*. Movement-related artefacts (mr-art) dataset of matched motion-corrupted and clean structural mri brain scans. *Scientific data* **9**, 630 (2022).
20. Duffy, B. A. *et al*. Retrospective motion artifact correction of structural MRI images using deep learning improves the quality of cortical surface reconstructions. *NeuroImage* **230**, 117756 (2021).
21. Knoll, F. *et al*. fastMRI: A Publicly Available Raw k-Space and DICOM Dataset of Knee Images for Accelerated MR Image Reconstruction Using Machine Learning. *Radiology: Artificial Intelligence* **2**, e190007 (2020).
22. Knudsen, G. M. *et al*. The center for integrated molecular brain imaging (cimbi) database. *NeuroImage* **124**, 1213–1219 (2016).
23. Gorgolewski, K. J. *et al*. The brain imaging data structure, a format for organizing and describing outputs of neuroimaging experiments. *Scientific Data* **3**, 160044 (2016).
24. Ganz, M. & Eichhorn, H. Datasets with and without deliberate head movements for evaluating the performance of markerless prospective motion correction and selective reacquisition in a general clinical protocol for brain MRI. https://doi.org/10.18112/openneuro.ds004332.v1.3.0 (2023).
25. Olesen, O. V., Paulsen, R. R., Hojgaard, L., Roed, B. & Larsen, R. Motion Tracking for Medical Imaging: A Nonvisible Structured Light Tracking Approach. *IEEE Transactions on Medical Imaging* **31**, 79–87 (2012).
26. Slipsager, J. M. *et al*. Markerless motion tracking and correction for PET, MRI, and simultaneous PET/MRI. *PLoS ONE* **14**, e0215524 (2019).
27. Eichhorn, H. Comparison of prospective and retrospective motion correction for magnetic resonance imaging of the brain - master's thesis in physics. https://osf.io/preprints/psyarxiv/jdfcv (2024).
28. Eichhorn, H. *et al*. Evaluating the performance of markerless prospective motion correction and selective reacquisition in a general clinical protocol for brain MRI. https://osf.io/vzh4g.
29. RealNoiseMRI - Grand Challenge. https://realnoisemri.grand-challenge.org/.
30. Skak Madsen, K., Ruschke, T., Eichhorn, H., Rising, P. & Ganz, M. Markerless Prospective Motion Correction Data. https://doi.org/10.70883/QBVI3432 (2025).
31. Fischl, B. Freesurfer. *NeuroImage* **62**, 774–781 (2012).
32. Greve, D. N. & Fischl, B. Accurate and robust brain image alignment using boundary-based registration. *NeuroImage* **48**, 63–72 (2009).
33. Reuter, M., Rosas, H. D. & Fischl, B. Highly accurate inverse consistent registration: A robust approach. *NeuroImage* **53**, 1181–1196 (2010).
34. Kecskemeti, S. *et al*. Robust Motion Correction Strategy for Structural MRI in Unsedated Children Demonstrated with Three-dimensional Radial MPnRAGE. *Radiology* **289**, 509 (2018).

Acknowledgements
This work was supported by the Elsass Foundation (18-3-0147). All MRI sequences with PMC were implemented by collaborators Robert Frost and André van der Kouwe (Athinoula A. Martinos Center for Biomedical Imaging, Massachusetts, US) and received via C2P. We thank research nurse Asta Kongsgaard for helping with recruitment and scanning. We also thank Bianca Pedersen and Martin Riis Rassing, the two radiographers responsible for the observer scores. Lastly, we extend our gratitude to Nitesh Shekhrajka as the radiologist rating the observer scores.

Author contributions
The study was conceptualized by Melanie Ganz and Kathrine Skak Madsen. Data acquisition was handled by Hannah Eichhorn and Melanie Ganz. Data analysis was performed by Hannah Eichhorn, Puk Rising, Tim Ruschke and Melanie Ganz. Lastly, all authors contributed to writing.

Competing interests
The authors declare no competing interests.

Additional information
Supplementary information The online version contains supplementary material available at https://doi.org/10.1038/s41597-026-07144-z.

Correspondence and requests for materials should be addressed to M.G.

Reprints and permissions information is available at www.nature.com/reprints.

Publisher's note Springer Nature remains neutral with regard to jurisdictional claims in published maps and institutional affiliations.

Open Access This article is licensed under a Creative Commons Attribution-NonCommercial-NoDerivatives 4.0 International License, which permits any non-commercial use, sharing, distribution and reproduction in any medium or format, as long as you give appropriate credit to the original author(s) and the source, provide a link to the Creative Commons licence, and indicate if you modified the licensed material. You do not have permission under this licence to share adapted material derived from this article or parts of it. The images or other third party material in this article are included in the article's Creative Commons licence, unless indicated otherwise in a credit line to the material. If material is not included in the article's Creative Commons licence and your intended use is not permitted by statutory regulation or exceeds the permitted use, you will need to obtain permission directly from the copyright holder. To view a copy of this licence, visit http://creativecommons.org/licenses/by-nc-nd/4.0/.

© The Author(s) 2026